

## ARTICLE

Received 13 May 2016 | Accepted 8 Sep 2016 | Published 19 Oct 2016

DOI: 10.1038/ncomms13152

OPEN

# Precise localization of metal nanoparticles in dendrimer nanosnakes or inner periphery and consequences in catalysis

Xiang Liu<sup>1,2</sup>, Danijela Gregurec<sup>3</sup>, Joseba Irigoyen<sup>3</sup>, Angel Martinez<sup>3</sup>, Sergio Moya<sup>3</sup>, Roberto Ciganda<sup>1,4</sup>, Philippe Hermange<sup>1</sup>, Jaime Ruiz<sup>1</sup> & Didier Astruc<sup>1</sup>

Understanding the relationship between the location of nanoparticles (NPs) in an organic matrix and their catalytic performances is essential for catalyst design. Here we show that catalytic activities of Au, Ag and CuNPs stabilized by dendrimers using coordination to intradendritic triazoles, galvanic replacement or stabilization outside dendrimers strongly depends on their location. AgNPs are found at the inner click dendrimer periphery, whereas CuNPs and AuNPs are encapsulated in click dendrimer nanosnakes. AuNPs and AgNPs formed by galvanic replacement are larger than precursors and only partly encapsulated. AuNPs are all the better 4-nitrophenol reduction catalysts as they are less sterically inhibited by the dendrimer interior, whereas on the contrary CuNPs are all the better alkyne azide cycloaddition catalysts as they are better protected from aerobic oxidation inside dendrimers. This work highlights the role of the location in macromolecules on the catalytic efficiency of metal nanoparticles and rationalizes optimization in catalyst engineering.

<sup>1</sup>ISM, UMR CNRS N°5255, Univ. Bordeaux, 33405 Talence, France. <sup>2</sup>UMR 6226, Institut des Sciences Chimiques de Rennes, CNRS-Université de Rennes 1, Campus de Beaulieu, 35042 Rennes, France. <sup>3</sup>CIC biomaGUNE, Unidad Biosuperficies, Paseo Miramon No. 182, Edif 'C', 20009 Donostia-San Sebastian, Spain. <sup>4</sup>Chemistry Department of San Sebastian, Basque Country University, Apdo. 1072, 20080 San Sebastian, Spain. Correspondence and requests for materials should be addressed to S.M. (email: smoya@cicbiomagune.es) or to D.A. (email: didier.astruc@u-bordeaux.fr).

Due to their unique physical and chemical properties transition metal nanoparticles (MNPs)<sup>1–4</sup> are being extensively used for numerous essential applications in catalysis<sup>4–13</sup>, energy storage and conversion<sup>14</sup>, magnetism<sup>2</sup>, optics<sup>1,3</sup> and biomedicine<sup>1,15</sup>. Among many types of MNP supports, macromolecules<sup>16,17</sup> and in particular dendrimers<sup>9,18–24</sup> have attracted considerable attention because of their encapsulation properties and the possibility to guide the formation of relatively well-defined very small MNPs. It is essential, however, to research the relationship between the MNP localization in macromolecules and their catalytic properties and performances. Following the discovery of MNP stabilization by dendrimers, the seminal works by Crooks' group<sup>9,18,19</sup> followed by others<sup>20–23</sup> have disclosed catalytic, electrocatalytic and sensing properties of PAMAM dendrimer-encapsulated NPs (DENs) and the functions of dendrimers as substrate nanofilters<sup>18,24</sup>. The discovery, design and nanoengineering of click dendrimers (CD), that is, synthesized by Cu(I)-catalysed alkyne azide cycloaddition (AAC)<sup>25–28</sup> and therefore containing intradendritic 1,2,3-triazolyl groups, has recently provoked a resurgence of interest for dendrimer-assisted MNP catalysis<sup>29–31</sup>. For instance it was shown that click-dendrimer-encapsulated PdNPs (Pd CDENs) using **1** catalyse useful cross C–C coupling reactions in only p.p.m. or sub-p.p.m. Pd amounts in aqueous media under ambient or mild conditions<sup>31</sup>. Although the encapsulation of MNPs inside dendrimers has been demonstrated by Crooks' groups<sup>18</sup>, the exact localization of MNPs in DENs still remained elusive<sup>32,33</sup>. Given the properties of MNPs<sup>1–4,33–37</sup>, the knowledge and understanding of this localization are important to optimize MNP engineering towards specific applications, and in particular catalysis. Here we report the relationship between the MNP localization and catalytic activity in 4-nitrophenol reduction (4-NP) to 4-aminophenol (4-AP) by NaBH<sub>4</sub> (refs 38–42) and CuNP-catalysed AAC reactions<sup>43</sup> of MNPs stabilized by either triazole-containing or triazole-free dendrimers. These new MNPs were synthesized following direct coordination of Cu(II), Ag(I) or Au(III) on intradendritic triazole followed by NaBH<sub>4</sub> reduction and by galvanic replacement<sup>9,18</sup> of the intradendritic CuNPs by Ag or Au upon redox reactions of the cations of the latter metals. The catalytic activities were also compared with those of group-11 MNPs that are stabilized, but not encapsulated by a structurally related ligand-free dendrimer.

Coordination of Cu(II), Ag(I) and Au(III) to intradendritic triazoles of a click dendrimer followed by reduction to metal (0) NPs is carried out here and shown by transmission electron microscopy (TEM) to form Cu, Ag and Au NPs. AgNPs are localized at the inner periphery of the dendrimer, however, whereas dendrimers containing the CuNPs and AuNPs form nanosnakes. The galvanic exchange of the CuNPs and AgNPs by AuNPs is shown to produce somewhat larger AuNPs that are not fully encapsulated inside the dendrimer. Finally CuNPs and AuNPs are also stabilized interdendrimerically by a related dendrimer that does not contain triazole ligands. These MNPs are characterized by UV–visible, X-ray photoelectron spectroscopy (XPS), TEM, scanning TEM (STEM), energy dispersive X-ray (EDX) and X-ray diffraction, and catalytic reactions are conducted herewith for 4-NP reduction by NaBH<sub>4</sub> to 4-AP and CuACC reactions. The conclusion drawn from this localization–reactivity relationship is specific to each type of catalysis with potential application of the disclosed principles to a variety of macromolecule-stabilized nanoparticle catalysts. For 4-NP reduction by NaBH<sub>4</sub> to 4-AP for which rearrangement of the AuNP surface is rate limiting, the steric effect around the AuNP surface is crucial, and catalysis by AuNPs located outside the dendrimer is shown to proceed much faster than catalysis by AuNPs stabilized at the interior of click dendrimers. Along the same line AgNPs that are also active catalysts for this reaction, although less so than AuNPs, are shown to be inactive when they are intradendrimerically stabilized. On the other hand for CuACC reactions, it is shown that the intradendrimerically protected CuNPs are much more efficient than the CuNPs stabilized interdendrimerically, because protection from air by the dendrimer framework is the crucial parameter that is considerably more favourable for the former CuNPs.

## Results

### Nanoparticles stabilized by a triazole-containing dendrimer.

Dendrimer **1** (Fig. 1a) that serves as MNP template contains 27 terminal triethylene glycol groups and was previously shown by dynamic light scattering to have a 9-nm size<sup>31</sup>, which is confirmed here by the TEM image<sup>33,34</sup> of its Au(III) complex synthesized by reaction of **1** with 9 equiv. HAuCl<sub>4</sub>·4H<sub>2</sub>O

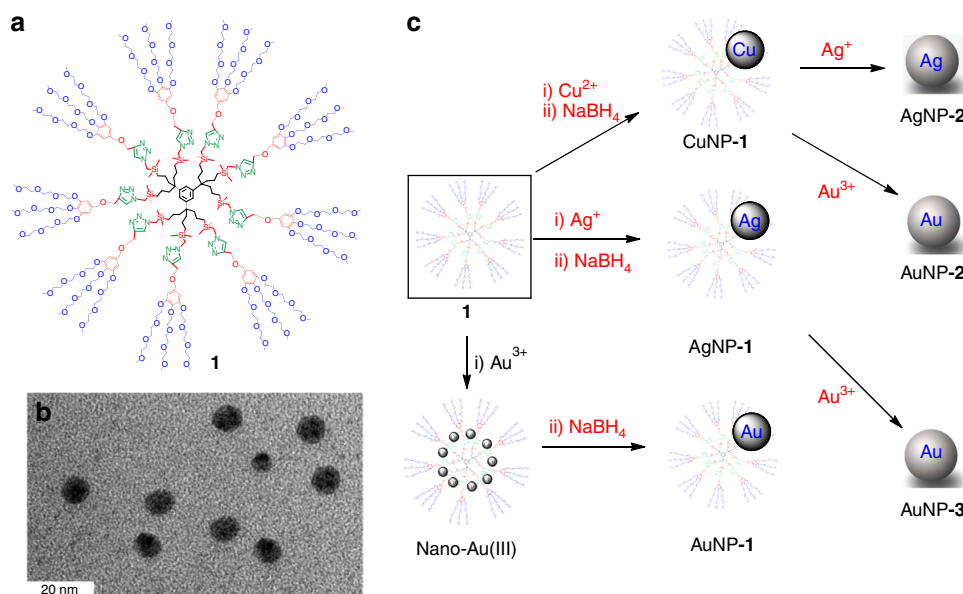


**Figure 1 | Formation of the group-11 metal NPs encapsulated and stabilized by the dendrimer **1**.** (a) Formula of dendrimer **1**; (b) TEM picture of the nona-Au(III) complex of **1**; (c) Syntheses of the metal CDENs and galvanic displacement reactions.

(Fig. 1b). The synthesis of the CDENs was conducted using water soluble salts of the metal ions and dendrimer **1** dissolved in deionized water in a standard molar ratio 1:1 of metal ion/triazole ligand followed by addition of the reductant  $\text{NaBH}_4$ .

The CuNP galvanic displacement reactions<sup>9,18</sup> were carried out by adding a stoichiometric amount of  $\text{AgNO}_3$  or  $\text{HAuCl}_4 \cdot 4\text{H}_2\text{O}$  to an aqueous 0.1 mM solution of Cu CDEN solution to form AgNP-2 or AuNP-2, or by adding a stoichiometric amount of  $\text{HAuCl}_4 \cdot 4\text{H}_2\text{O}$  to an aqueous 0.1 mM solution of Ag CDENs solution to form AuNP-3 (Fig. 1c).

The TEM picture shows encapsulation of the Cu, Ag and Au nanoparticles, but interestingly the case of the AgNPs is different from those of the CuNPs and AuNPs, that is, these AgNPs-1 are localized at the inner periphery of the dendrimer **1** (Fig. 2a), whereas the dendrimers **1** that encapsulate CuNPs-1 and AuNPs-1 form nanosnakes (Fig. 2b,c). The localization of the AgNPs-1 at the inner periphery of **1** is also visible in the STEM image of AgNP-1 (Fig. 3a). The dendrimers that encapsulate the AgNP-1 also have a size of 9 nm (TEM, grey spheres in Fig. 2a and Supplementary Fig. 1) matching the size of **1** (dynamic light scattering)<sup>31</sup> and its Au(III) complex (Fig. 1b; Supplementary Fig. 2) and Ag(I) (Supplementary Fig. 3) complexes. The CDEN AgNP-1 located at the inner periphery of **1** have a core size of 3.5 nm and a surface plasmon band (SPB) at 425 nm in the UV-visible spectrum (Fig. 3e). This size corresponds to 1,340 Ag atoms, which means that many dendrimers **1** do not contain AgNPs. This is verified in the EDX analysis compositional map of Ag by the presence of large black areas (Fig. 3b) and in the combined (Ag, C and Si) compositional map by the large green and blue dendrimer zones representing carbon resp. silicon atoms without the red spots representing the AgNPs (Fig. 3c). Such a situation is characteristic of Ostwald ripening<sup>44</sup>, that is, of migration of Ag atoms among dendrimers and contrasts with the previous formation of click Pd CDEPs without significant Pd atom escape<sup>29</sup>. It may also be specific of click dendrimers terminated by triethylene glycol groups for these metals, whereas the well-known PAMAM DENs were shown by Crooks' group

to contain essentially all group-10 and group-11 metal atoms generated by reduction of their amine-coordinated cations inside the PAMAM dendrimers<sup>18</sup>. To complete the characterization AgNP-1, XPS (Fig. 3d) was recorded, showing peaks at 368.1 and 374.5 eV that correspond to  $3d_{5/2}$  and  $3d_{3/2}$  core levels of metallic silver, respectively. The binding energy of 368.1 eV for Ag  $3d_{5/2}$  assigned to AgNPs shows that the surface atoms of AgNP-1 are exclusively zero valent.

CuNP-1 and AuNP-1 also follow this same trend involving Oswald ripening as the size of their CDENs formed here by direct intradendritic triazole coordination followed by  $\text{NaBH}_4$  reduction have sizes of 2.0 and 4.5 nm, respectively (Supplementary Figs 4 and 5). Their TEM images are reproducibly in sharp contrast with that of AgNP-1, as these dendrimers appear to form nanosnake networks that encapsulate the MNPs (Fig. 2b,c). The triethylene glycol termini may play the role of a supramolecular glue binding the dendrimers to one another although monodimensionality is preferred in contrast to the dendrimers encapsulating AgNP-1 that do not agglomerate. The STEM image of CuNP-1 shown in Fig. 2d confirms that the CuNPs are encapsulated by nanosnake networks formed by the dendrimer molecules.

Galvanic replacement of CuNP by more noble metals<sup>18</sup>, that is, metals that have more positive oxidation potentials, was achieved by reactions of the Cu CDENs with the salts of these noble metals and led to 10.9 nm sized dendrimer-stabilized AgNP-2 (Supplementary Fig. 6) and 5.1 nm sized AuNP-2 (Supplementary Fig. 7), respectively, whereas replacement of AgNP-1 by Au carried out by reaction with  $\text{HAuCl}_4 \cdot 4\text{H}_2\text{O}$  led to 4.5 nm-sized dendrimer-stabilized AuNP-3 (Supplementary Fig. 8). The fact that AgNP-2 is much larger than CuNP-1 shows that redox exchange proceeds along with considerable NP rearrangement and that the resulting AgNP-2 are no longer encapsulated in the dendrimer **1**, but stabilized by several dendrimer molecules. The galvanic exchange producing AuNP-2 and AuNP-3 proceeds with some size increase so that the resulting AuNPs cannot be fully encapsulated inside the dendrimer. This situation contrasts with that encountered with PAMAM DENs that undergo *in situ* displacement reactions<sup>9,18</sup>.

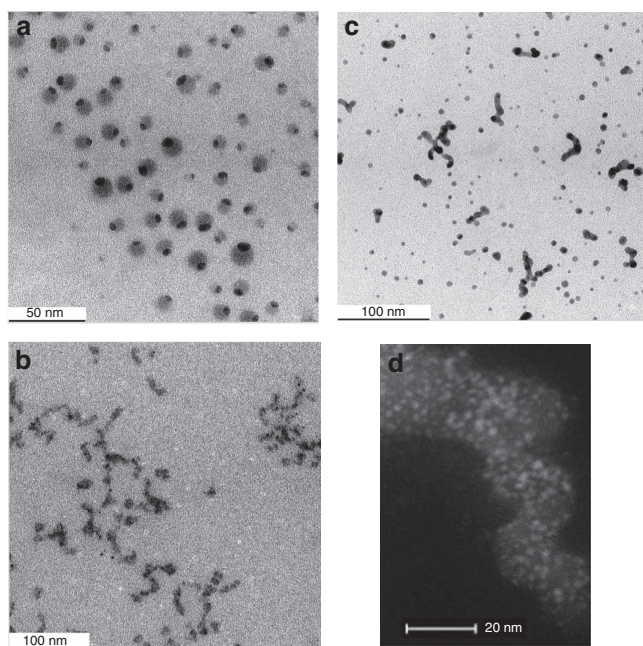


**Figure 2 | Microscopy images of the group-11 metal NPs intradendritically encapsulated by dendrimer **1**.** (a) TEM image of AgNP-1; (b) TEM image of CuNP-1; (c) TEM image of AuNP-1; (d) STEM image of CuNP-1.

**Nanoparticles stabilized by a triazole-free dendrimer.** To compare the behaviour of DENs with that of NPs stabilized outside dendrimers, the new water-soluble dendrimer **2** (Fig. 4) was synthesized from the same nona-allyl core that led to **1** (for more information, see Supplementary Methods). Thus dendrimer **2** resembles **1** with 27 termini but does not contain ligands, unlike **1**. Stabilization of CuNP-2 (4.3 nm) and AuNP-4 (6.6 nm) by dendrimer **2** upon  $\text{NaBH}_4$  reduction of the group-11 metal cations then occurs by interactions with several dendrimer molecules (Fig. 4). The core sizes and SPBs of all the NPs stabilized by dendrimer **1** or dendrimer **2** are gathered in Table 1.

The goal of these syntheses was to compare the catalytic performances of CuNP-2 (Supplementary Fig. 9) and AuNP-4 (Supplementary Fig. 10) located outside dendrimer **2**, with the NPs that are encapsulated in the dendrimer interior of **1** or partly penetrating into **1**. CuNP-2 is considerably more easily oxidized than the CDEN CuNP-1 to  $\text{Cu}_2\text{O}$  outside **2** as indicated by fast colour change from light yellow (Fig. 5c) to dark green (Fig. 5d) and the new absorption at 352 nm characteristic of  $\text{Cu}_2\text{O}$  (ref. 45) appearing after 5 min (Fig. 5d). This oxidability of CuNP-2 indeed greatly contrasts with that of CuNP-1 that is fully stable as Cu(0) for at least two months as shown by UV-visible (Fig. 5a,b).

The presence of only Cu(0) in CuNP-1 is confirmed by the XPS as X-ray diffraction spectra. In XPS, CuNP-1 (Fig. 6a) does not show shake up features characteristic of oxidized Cu at 943 and



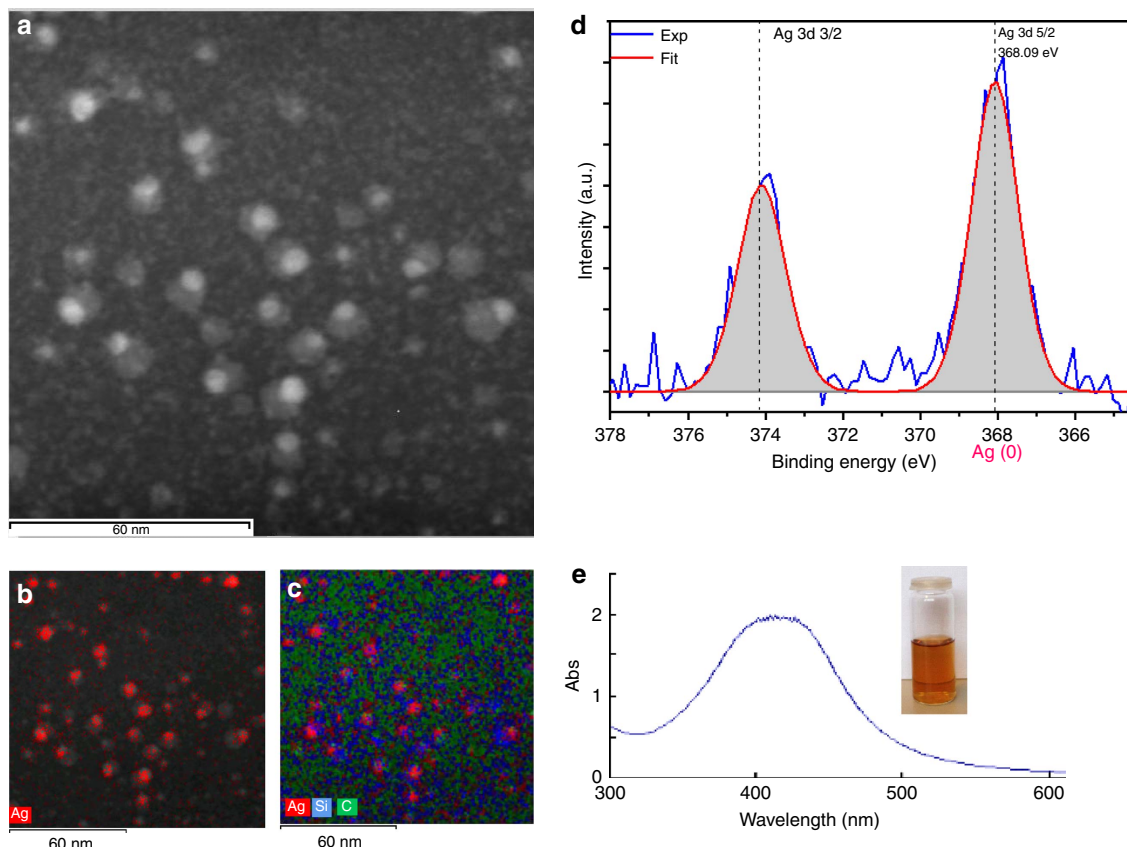


**Figure 3 | Microscopy images and spectra for AgNP-1.** (a) STEM image of AgNP-1; (b) Ag EDX compositional map of AgNP-1; (c) combined (Ag, Si and C) EDX compositional map; (d) XPS of AgNP-1; (e) UV-visible spectrum (SPB at 425 nm) and photograph of AgNP-1.

963.5 eV. So the XPS spectrum clearly confirms Cu(0) chemical state alone. If Cu (I) would be present, a weak satellite features would be recorded at these energies, which is not the case here<sup>46</sup>. The X-ray diffraction of CuNP-1 (Fig. 6c) shows its long-term aerobic stability as Cu(0). The finding that CuNP-1 are at the oxidation state Cu(0) is logical, because their surface is only bonded to neutral triazole ligands, and it just means that the dendrimer framework is protecting inside the dendrimer interior against intradendritic aerobic CuNP oxidation. On the other hand, CuNP-2 appears to be in the form of a mixture of Cu(0), Cu<sub>2</sub>O and CuO. Indeed, in the XPS spectrum of CuNP-2 (Fig. 6b) is resolved to at least two states. The main peak at 933.4 and 952.0 eV correspond to  $2p_{3/2}$  and  $2p_{1/2}$  core levels of Cu(0). The pronounced shake up features at binding energies of 941.29 and 944.93 eV shows oxidation to Cu(I) or (II)<sup>47</sup>. Moreover Cu(II) is confirmed by detailed examination of line shape and shake up satellite feature found at 963.25 eV being characteristic of only Cu (II) thus confirming oxidation of Cu NP-2 all the way to CuO (for detailed discussion, see Supplementary Discussion).<sup>46</sup> This spectrum also shows peaks at 933.4 and 952.0 eV that correspond to  $2p_{3/2}$  and  $2p_{1/2}$  core levels of Cu(0). The X-ray diffraction spectrum of CuNP-2 is shown in Fig. 6d. The peaks (1 1 0) (29.5 eV), (1 1 1) (36.4 eV), (2 0 0) (42.3 eV), (2 2 0) (61.6 eV) and (3 1 1) (73.8 eV) belong to Cu<sub>2</sub>O, and the other peaks at (111) (43.5 eV), (200) (50.4 eV) and (220) (74.0 eV) planes belong to metallic Cu (0). CuNP-2 are not protected inside the dendrimer and are thus considerably more exposed to aerobic oxidation as witnessed by the dramatic fast colour change within 5 min and the above spectroscopic data. This means that the inside of CuNP-2 remain in the Cu(0) state, whereas the exposed surface Cu atoms are oxidized to Cu<sub>2</sub>O and CuO.

**Catalysis.** To compare the catalytic properties of these CDENs with those of NPs that are not encapsulated in the dendrimer 1, but stabilized by several molecules of dendrimer 1, two catalytic reactions have been conducted in water: (i) the AuNP-catalysed 4-NP reduction to 4-AMP (Fig. 7, equation (1)), and (ii) the CuNP-catalysed AAC ‘click’ reaction selectively giving a 1,4-diphenyl-1,2,3-triazole (Fig. 7, equation (2)).

First, the AuNP-catalysed 4-NP reduction is representative<sup>38–42</sup>, being highly sensitive to the catalyst surface environment with the Langmuir-Hinshelwood mechanism highlighted by Ballauff’s group<sup>38,39</sup>. In this mechanism, both reactant molecules, 4-nitrophenol and borohydride, are adsorbed on adjacent sites of the NP surface before the reaction, and this reaction takes place via an activated complex on the NP surface involving NP surface reconstruction. Its kinetics is conveniently monitored by UV-visible spectroscopic analysis with absorptions at  $\lambda = 400$  and 300 nm corresponding to 4-NP and 4-AP, respectively, and characterized by the disappearance of the yellow colour of 4-NP upon reduction. This reaction has been carried out with 100 equiv. of NaBH<sub>4</sub> in water in the presence of 0.5 mol% resp. 2.0 mol% AuNP-1 (as shown in Supplementary Table 1). This catalysis by AuNP-1 was found to be slow and to require an induction time of 480 s resp. 180 s due to the reorganization at the catalyst surface. This induction time is taken into account by the encapsulation of the AuNP-1 (CDENs) inside nanosnakes (Fig. 2c) that provides partial steric inhibition of the substrate access to the AuNP surface<sup>38–40</sup>. On the other hand AuNP-4 located outside dendrimer 2 without steric inhibition of the dendrimer encapsulation clearly benefits from easier access to the AuNP surface. Indeed no induction time is found, and the 4-NP rate constant is large. The cases of dendrimer-1-stabilized AuNP-2 and AuNP-3 are intermediate between those of AuNP-1 and AuNP-4.

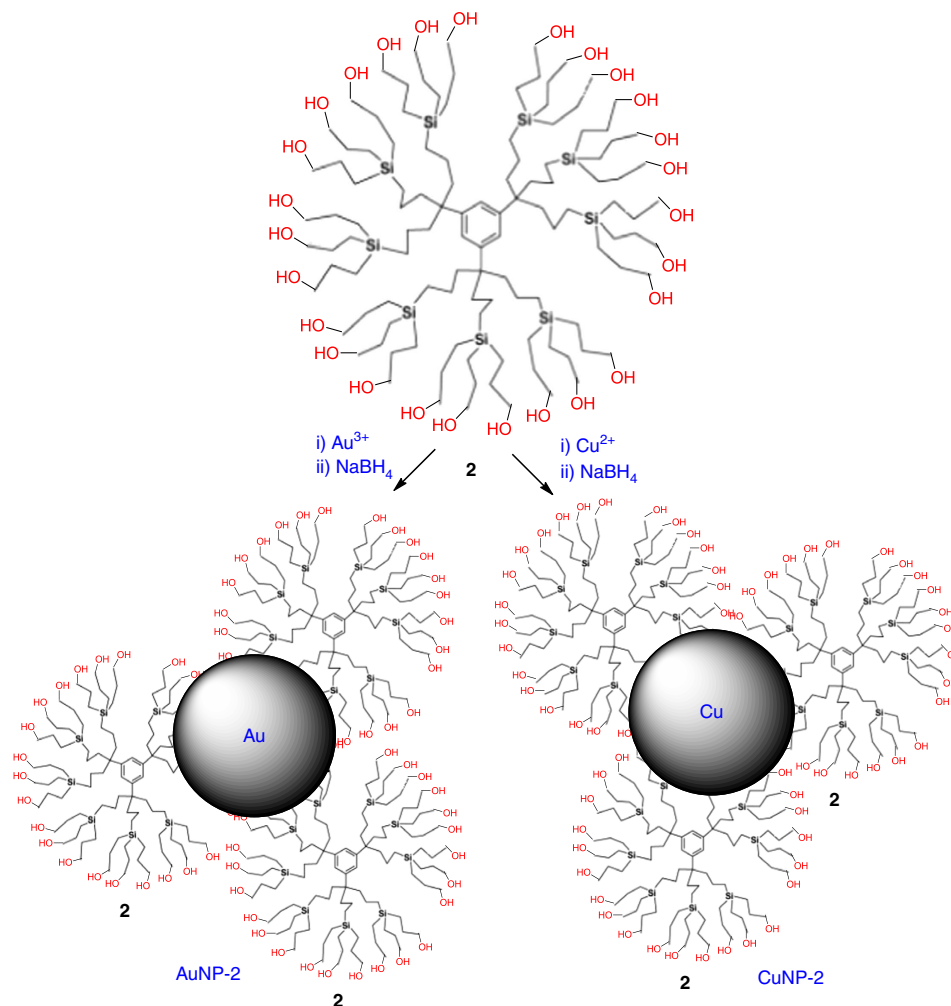


**Figure 4 | Synthesis of AuNP-2 and CuNP-2.** The lack of intradendritic ligands in dendrimer **2** induces the formation of large TMNPs AuNP-2 and CuNP-2 stabilized by clusters of dendrimers.

**Table 1 | SPBs and core sizes of all the NPs.**

| MNPs   | SPB (nm)  | Diameter (nm)  |
|--------|-----------|----------------|
| CuNP-1 | —         | $2.0 \pm 0.1$  |
| CuNP-2 | 352*, 626 | $4.3 \pm 0.1$  |
| AgNP-1 | 425       | $3.5 \pm 0.1$  |
| AgNP-2 | 425       | $10.9 \pm 0.2$ |
| AuNP-1 | 512       | $4.5 \pm 0.1$  |
| AuNP-2 | 540       | $5.1 \pm 0.1$  |
| AuNP-3 | 527       | $4.5 \pm 0.1$  |
| AuNP-4 | 520       | $6.6 \pm 0.2$  |

\*The band at 352 nm is due to  $\text{Cu}_2\text{O}$  (ref. 45).  
For CuNP-1, no SPB is observable due to its subplasmonic core size.

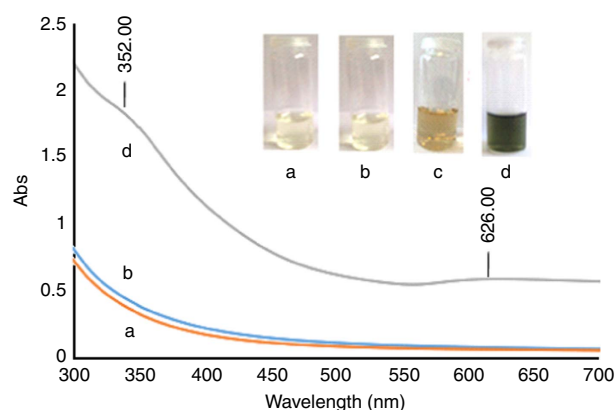


**Figure 5 | Compared photographs and UV-visible spectra of CuNP-1 and CuNP-2 upon standing in air.** (a) Photograph and UV-visible spectrum of CuNP-1 after 1 min; (b) photograph and UV-visible spectrum of CuNP-1 after 2 months; (c) photograph of CuNP-2 after 1 min; (d) photograph and UV-visible spectrum of CuNP-2 after 5 min.

They partly penetrate dendrimer **1** in contact with the intradendritic triazoles, but they are too large for full intradendritic encapsulation into a single dendrimer. They exhibit part of their surface outside dendrimer **1** allowing more efficient catalysis than inside dendrimer **1** but less efficient catalysis than AuNP-4 that is not attracted by triazole ligands in the dendrimer interior. Along this line and accordingly, CuNP-1 and AgNP-1 that are CDENs do not catalyse 4-NP reduction under these conditions even in the presence of high catalyst amounts (the yellow colour of the

solution does not disappear in two months), obviously also due to steric inhibition resulting from the encapsulation, whereas other CuNPs and AgNPs are known 4-NP reduction catalysts under ambient conditions<sup>41,47</sup>.

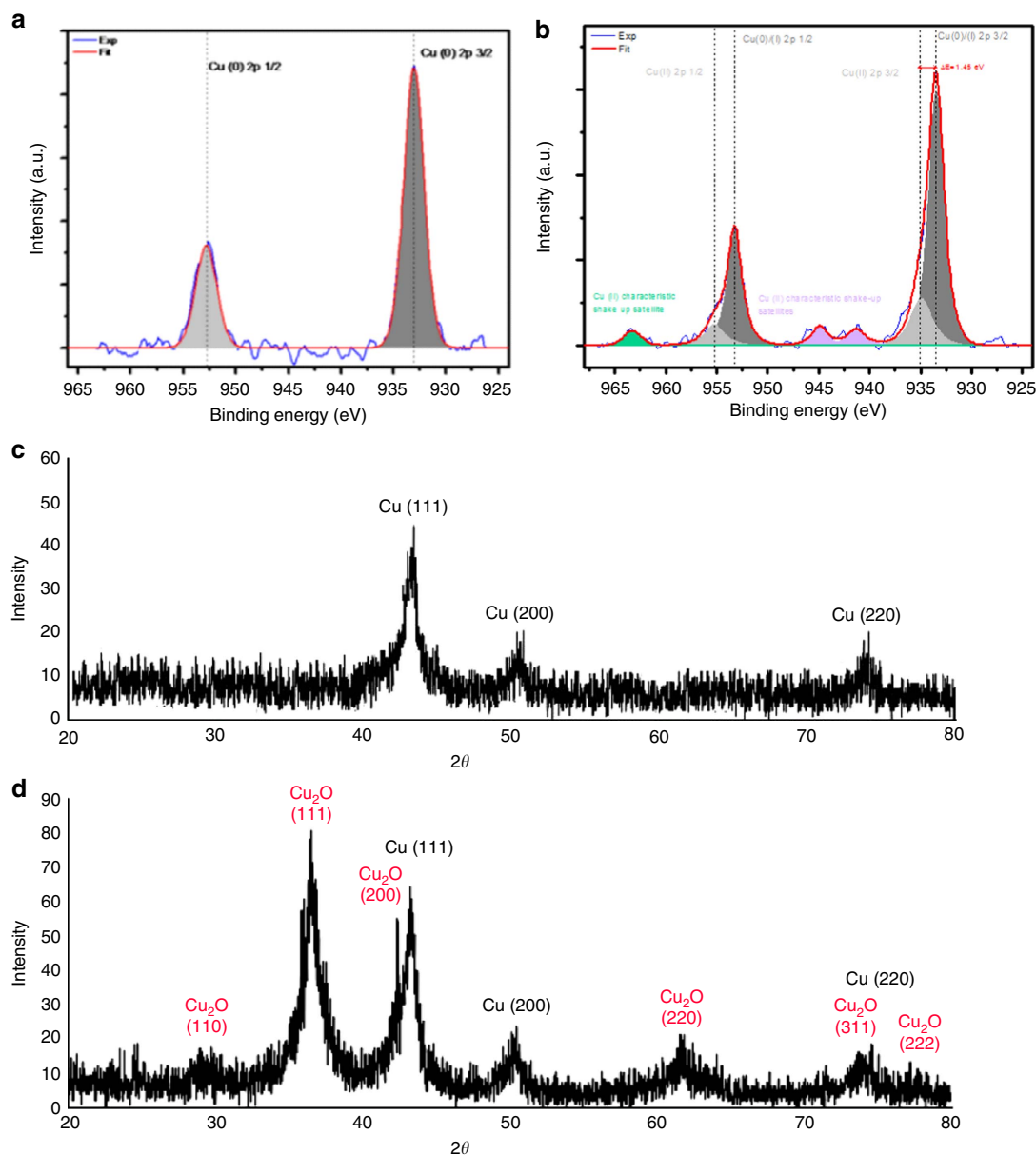


**Figure 6 | XPS and X-ray diffraction spectra of CuNP-1 and CuNP-2.** (a) XPS spectrum of CuNP-1 showing its long-term aerobic stability as Cu (0); (b) XPS spectrum of CuNP-2 showing its oxidation as Cu (I) and Cu (II); (c) X-ray diffraction spectrum of CuNP-1 showing that only Cu (0) is present; (d) X-ray diffraction spectrum of CuNP-2 showing the presence of both Cu (0) and Cu<sub>2</sub>O.

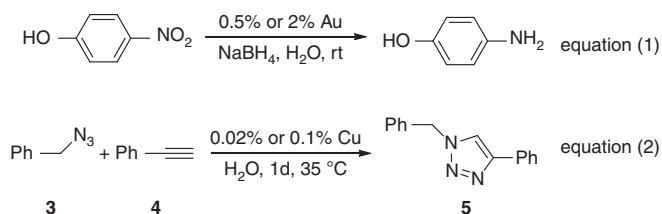


**Figure 7 | Catalytic reactions conducted with the AuPs and CuNPs as catalysts.** In equation (1), the 4-NP reduction to 4-AP by NaBH<sub>4</sub> is catalysed by AuNPs, and in equation (2) the copper-catalysed azide alkyne cycloaddition (CuAAC, click reaction) is catalysed by CuNPs.

The second test reaction allowing a key comparison between the dendrimer-stabilized MNP catalysts—the CuAAC reaction between **3** and **4** selectively yielding **5** (Fig. 7, equation (2))<sup>28</sup>—

was conducted using either the CDEN CuNP-1 or the dendrimer-stabilized CuNP-2 as catalyst.

Optimized reaction between **3** (0.55 mmol) and **4** (0.5 mmol) catalysed by CuNP-1 (200 resp. 1,000 p.p.m. Cu) and 2 ml H<sub>2</sub>O for 24 h at 35 °C under N<sub>2</sub> yielded 45% resp. 100% of **5**, but with CuNP-2 the catalytic activity is poor, the yield being only 9% resp. 15% (equation (2) and Supplementary Fig. 11). This difference is best taken into account by the fact that the click reaction is strongly activated by intradendritic triazole ligands, whereas for CuNP-2 outside dendrimer **2** and without triazole ligands no activation occurs. Interestingly note that CuNP-1 has a pure Cu(0) state (*vide supra*), whereas for CuNP-2, the oxidation state I that was observed (*vide supra*) is usually favourable for CuAAC catalysis. There are a number of precedents for Cu metal or CuNP AAC catalysis<sup>43</sup>, and the present data confirm the efficiency of non-oxidized, but triazole-ligated Cu(0) nanoparticles. In this type of catalysis, the intradendritic protection and ligand

activation are essential to inhibit the formation of oxidized CuNPs outside dendrimers and activate CuAAC catalysts.

## Discussion

The new CuNP-1 and AuNP-1 that are encapsulated by 'click' dendrimer 1 terminated by triethylene glycol groups have been shown to form nanosnakes for Cu and Au, the triethylene glycol termini providing supramolecular interdendritic 1D interactions that act as a glue. On the other hand, remarkably, AgNP-1 are localized at the inner periphery of click dendrimers. Their galvanic replacement reactions yield AuNP-2, AuNP-3 and AgNP-2 that are larger and no longer encapsulated in dendrimers but only partly penetrating into the dendrimers. With a similar triazole-free dendrimer 2, CuNP-2 and AuNP-4 are only stabilized outside the dendrimer.

A correlation is then established between the catalytic activities of these MNPs and their localization, that is, inside versus partly outside the click dendrimer 1 or outside the non-click dendrimer 2. The encapsulation of these Cu, Ag and Au NPs inside the click dendrimer 1 sterically inhibits the access to the AuNP-1 surface slowing down the catalysis of 4-NP reduction and provoking an induction time for the reorganization of the NP surface environment. Under identical conditions, AuNP-2 and AuNP-3 resulting from galvanic replacement and located partly outside the click dendrimers and are less subjected to steric inhibition nor catalytic induction time and are better 4-NP reduction catalysts. Finally, AuNP-4 stabilized outside the non-click dendrimer are the most efficient catalysts as a result of minimal steric inhibition of the catalytic surface.

On the contrary, catalysis of the CuAAC 'click' reaction by intradendritically encapsulated and triazole-activated CuNP-1 is efficient, providing quantitative yield of the 1,4-disubstituted triazole with 0.1 mol% Cu, because they are protected from aerobic oxidation, whereas CuNP-2 located outside dendrimers are very rapidly oxidized at their surface and are a very poor click catalyst. In this case, the catalytic reactivity is directed by the system ability to prevent the first-row transition metal NPs from oxidation. On the other hand, air stable AuNPs are not sensitive to this parameter, and their activity is only linked to the intradendritic steric surface inhibition. This type of correlation of NP localization vs. catalytic activity in nanomaterials, that is specific to the type of reaction and of MNPs, is essential for MNP catalyst engineering towards a greener chemistry<sup>48</sup>.

## Methods

**Preparation of NPs encapsulated in the dendrimer 1.**  $3.6 \times 10^{-4}$  mmol of dendrimer 1 (2.59 mg) is dissolved in 1.1 ml of water in a Schlenk flask, and a colourless solution of  $\text{CuSO}_4 \cdot 5\text{H}_2\text{O}$ ,  $\text{AgNO}_3$  or  $\text{HAuCl}_4 \cdot 4\text{H}_2\text{O}$  ( $3.2 \times 10^{-3}$  mmol in 1.1 ml water) is added to the solution of the dendrimer. Thirty millilitre of water is added, and the solution is stirred for 1 h. The concentration of Cu(II), Ag(I) or Au(III) is 0.1 mM. A 1-ml aqueous solution containing  $3.2 \times 10^{-2}$  mmol of  $\text{NaBH}_4$  is added dropwise, provoking the formation of a yellow (CuNP-1), orange (AgNP-1) or purple (AuNP-1) colour (Fig. 2c) corresponding to the reduction of the cation to the zero-valent metal and MNP formation. A plasmon band is observed in the UV-visible spectra only for AgNP-1 (425 nm) and AuNP-1 (512 nm).

**Preparation of dendrimer-MNPs by galvanic displacement.** A concentration of  $3.6 \times 10^{-4}$  mmol of dendrimer 1 (2.59 mg) is dissolved in 1.1 ml of water in a Schlenk flask, and a colourless solution of  $\text{CuSO}_4 \cdot 5\text{H}_2\text{O}$  ( $3.2 \times 10^{-3}$  mmol in 1.1 ml water) is added to the solution of the dendrimer. Thirty millilitre of water is added, and the solution is stirred for 1 h. The concentration of Cu(II) is 0.1 mM. A 1 ml aqueous solution containing  $6.4 \times 10^{-3}$  mmol of  $\text{NaBH}_4$  is added dropwise, provoking the formation of a yellow colour (Fig. 2b) corresponding to the reduction of Cu(II) to Cu(0) and formation of CuNP-1. The dendrimer 1-encapsulated CuNP-1 solution is purged with  $\text{N}_2$  continuously for 15 min before addition of  $\text{NaBH}_4$  until 2 h after reduction. A borohydride destruction procedure follows by addition of aqueous  $\text{HClO}_4$ , the pH of the resulting 0.1 mM CuNP solution being adjusted to 3. Then a colourless solution of  $\text{AgNO}_3$  ( $3.2 \times 10^{-3}$  mmol in 1.1 ml water) is added dropwise to the solution of the

dendrimer-1, provoking the formation of an orange colour corresponding to the reduction of Ag(I) to Ag(0) by CuNP-1. The formation of AgNP-2 is characterized by a plasmon band at 425 nm in the UV-visible spectrum. AuNP-2 and AuNP-3 are similarly synthesized by galvanic displacement from CuNP-1 resp. AgNP-1.

**Preparation of AuNP-4 and CuNP-2 stabilized by dendrimer 2.** A concentration of  $3.6 \times 10^{-4}$  mmol of dendrimer 2 (0.8 mg,  $3.6 \times 10^{-4}$  mmol) is dissolved in 1.1 ml of water in a Schlenk flask, and a colourless solution of  $\text{CuSO}_4 \cdot 5\text{H}_2\text{O}$  or  $\text{HAuCl}_4 \cdot 4\text{H}_2\text{O}$  ( $9.72 \times 10^{-3}$  mmol in 1.1 ml water) is added to the solution of the dendrimer. Thirty millilitre of water is added, and the solution is stirred for 1 h. The concentration of Cu(II) or Au(III) is 0.1 mM. A 1-ml aqueous solution containing  $9.72 \times 10^{-2}$  mmol of  $\text{NaBH}_4$  is added dropwise, provoking the formation of a green (CuNP-2) or purple (AuNP-4) colour (Supplementary Fig. 10) corresponding to the reduction of the cation to the zero-valent metal and MNP formation. A plasmon band is observed in the UV-visible spectra only for CuNP-2 (352 nm, 628 nm) (Supplementary Fig. 9) and AuNP-4 (520 nm) (Supplementary Fig. 10).

**Catalysis of 4-nitrophenol reduction.** An aqueous solution (2.5 ml) containing 4-nitrophenol (0.09 mmol) and  $\text{NaBH}_4$  (7.2 mmol) is prepared in a standard quartz cuvette (3 ml, path length: 1 cm). The AuNP catalyst (0.5 mol%,  $0.45 \times 10^{-3}$  mmol) is injected into this solution, and the reaction progress is detected by UV-visible spectroscopic analysis every min at 22 °C (Supplementary Figs 12–19).

**CuAAC reaction leading to the triazole derivative 5.** Benzyl azide (3) 0.5 mmol, ethynylbenzene (4) 0.55 mmol, CuNP-2 (0.1% mmol) and 2 ml  $\text{H}_2\text{O}$  are taken in a round bottom flask equipped with a magnetic stirrer. The resulting mixture is stirred for 24 h at 35 °C under  $\text{N}_2$ . After cooling to room temperature, water (2 ml) is added to the reaction mixture, and the latter is extracted with ethyl acetate ( $3 \times 10$  ml). The combined organic phases are washed with brine ( $2 \times 5$  ml), dried over anhydrous  $\text{MgSO}_4$  and concentrated *in vacuo*. The residue is subjected to flash column chromatography with hexanes/EtOAc (v/v = 5/1) as eluent to obtain the desired 1-benzyl-4-phenyl-1H-1,2,3-triazole (5) as a white solid (100% yield).

**Data availability.** All data is available from the authors upon reasonable request.

## References

- Schmid, G. (ed.) *Nanoparticles: From Theory to Application*. (Wiley-VCH, 2004).
- Xia, Y. N., Xiong, Y. J., Lim, B. & Skrabalak, S. E. Shape-controlled synthesis of metal nanocrystals: simple chemistry meets complex physics? *Angew. Chem. Int. Ed. Engl.* **48**, 60–103 (2009).
- Brongersma, M. L., Halas, N. J. & Nordlander, P. Plasmon-induced hot carrier science and technology. *Nat. Nanotechnol.* **10**, 25–34 (2015).
- Daniel, M.-C. & Astruc, D. Gold nanoparticles: assembly, supramolecular chemistry, quantum-size-related properties, and applications toward biology, catalysis, and nanotechnology. *Chem. Rev.* **104**, 293–346 (2004).
- Haruta, M. & Date, M. Advances in the catalysis of Au nanoparticles. *Appl. Catal. A-Gen.* **222**, 427–437 (2001).
- Sankar, M. *et al.* Designing bimetallic catalysts for a green and sustainable future. *Chem. Soc. Rev.* **41**, 8099–8139 (2012).
- Corma, A. & Garcia, H. Supported gold nanoparticles as catalysts for organic reactions. *Chem. Soc. Rev.* **37**, 2096–2126 (2008).
- Joo, S. H. *et al.* Thermally stable Pt/mesoporous silica core-shell nanocatalysts for high-temperature reactions. *Nat. Mater.* **8**, 126–131 (2009).
- Myers, V. S. *et al.* Dendrimer-encapsulated nanoparticles: new synthetic and characterization methods and catalytic applications. *Chem. Sci.* **2**, 1632–1646 (2011).
- Hervés, P. *et al.* Catalysis by metallic nanoparticles in aqueous solution: model reactions. *Chem. Soc. Rev.* **41**, 5577–5587 (2012).
- Fihri, A., Bouhrara, M., Nekoueiahraki, B., Basset, J. M. & Polshettiwar, V. Nanocatalysts for Suzuki cross-coupling reactions. *Chem. Soc. Rev.* **40**, 5181–5203 (2011).
- Bronstein, L. M. & Shifrina, Z. B. Dendrimers as encapsulating, stabilizing, or directing agents for inorganic nanoparticles. *Chem. Rev.* **111**, 5301–5344 (2011).
- Astruc, D., Lu, F. & Ruiz, J. Nanoparticles as recyclable catalysts: the Frontier between homogeneous and heterogeneous catalysis. *Angew. Chem. Int. Ed. Engl.* **44**, 7852–7872 (2005).
- Kai, Z., Han, X. & Hu, Z. Nanostructured Mn-based oxides for electrochemical energy storage and conversion. *Chem. Soc. Rev.* **44**, 699–728 (2015).
- Dreaden, E. C., Alkilany, A. M., Huang, X. H., Murphy, C. J. & El Sayed, M. A. The golden age: gold nanoparticles for biomedicine. *Chem. Soc. Rev.* **41**, 2740–2779 (2012).
- Toshima, N. & Yonezawa, T. Bimetallic nanoparticles-novel materials for chemical and physical applications. *New J. Chem.* **22**, 1179–1201 (1998).



17. Wang, X. *et al.* Cylindrical block copolymer micelles and co-micelles of controlled length and architecture. *Science* **317**, 644–647 (2007).
18. Crooks, R. M., Zhao, M. Q., Sun, L., Chechik, V. & Yeung, L. K. Dendrimer-encapsulated metal nanoparticles: synthesis, characterization, and applications to catalysis. *Acc. Chem. Res.* **34**, 181–190 (2001).
19. Anderson, R. M. *et al.* A theoretical and experimental approach for correlating nanoparticle structure and electrocatalytic activity. *Acc. Chem. Res.* **48**, 1351–1357 (2015).
20. Li, Y. & El-Sayed, M. A. The effect of stabilizers on the catalytic activity and stability of Pd colloidal nanoparticles in the Suzuki reactions in aqueous solution. *J. Chem. Phys. B* **105**, 8938–8943 (2001).
21. Lang, H. F., May, R. A., Iversen, B. L. & Chandler, B. D. Dendrimer-encapsulated nanoparticle precursors to supported platinum catalysts. *J. Am. Chem. Soc.* **125**, 14832–14836 (2003).
22. Gross, E., Liu, J. H.-C., Toste, F. D. & Somorjai, G. A. Control of Selectivity by tuning nanoparticle properties and reactor residence time. *Nat. Chem.* **4**, 947–952 (2012).
23. Wang, D., Deraedt, C. & Astruc, D. Magnetic and dendritic catalysts. *Acc. Chem. Res.* **48**, 1871–1880 (2015).
24. Niu, Y. H., Yeung, L. K. & Crooks, R. M. Size-selective hydrogenation of olefins by dendrimer-encapsulated palladium nanoparticles. *J. Am. Chem. Soc.* **123**, 6840–6846 (2001).
25. Wu, P. *et al.* Efficiency and fidelity in a click-chemistry route to triazole dendrimers by the copper(I)-catalyzed ligation of azides and alkynes. *Angew. Chem. Int. Ed. Engl.* **43**, 3928–3932 (2004).
26. Ornelas, C., Ruiz, J., Cloutet, E. & Astruc, D. Click assembly of 1,2,3-triazole-linked dendrimers, including ferrocenyl dendrimers, which sense both oxo anions and metal cations. *Angew. Chem. Int. Ed. Engl.* **46**, 872–877 (2007).
27. Franc, G. & Kakkar, A. K. 'Click' methodologies: efficient, simple and greener routes to design dendrimers. *Chem. Soc. Rev.* **39**, 1536–1544 (2010).
28. Arseneault, M., Wafer, C. & Morin, J.-F. Recent advances in click chemistry applied to dendrimer synthesis. *Molecules* **20**, 9263–9294 (2015).
29. Diallo, A. K., Ornelas, C., Salmon, L., Ruiz, J. & Astruc, D. 'Homeopathic' catalytic activity and atom-leaching mechanism in Miyaura–Suzuki reactions under ambient conditions with precise dendrimer-stabilized Pd nanoparticles. *Angew. Chem. Int. Ed. Engl.* **46**, 8644–8648 (2007).
30. Astruc, D., Liang, L., Rapakousiou, A. & Ruiz, J. Click dendrimers and triazole-related aspects: catalysts, mechanism, synthesis, and functions. A bridge between dendritic architectures and nanomaterials. *Acc. Chem. Res.* **45**, 630–640 (2012).
31. Deraedt, C., Pinaud, N. & Astruc, D. Recyclable catalytic dendrimer nanoreactor for part-per-million Cu(I) catalysis of 'Click' chemistry in water. *J. Am. Chem. Soc.* **136**, 12092 (2014).
32. Gomez, V., Guerra, J., Velders, A. H. & Crooks, R. M. NMR characterization of fourth-generation PAMAM dendrimers in the presence and absence of palladium dendrimer-encapsulated nanoparticles. *J. Am. Chem. Soc.* **131**, 341–350 (2009).
33. Gröhn, F., Bauer, B. J., Akpalu, Y. A., Jackson, C. L. & Amis, E. J. Dendrimer templates for the formation of gold nanoclusters. *Macromolecules* **33**, 6042–6050 (2000).
34. Jackson, C. L. *et al.* Visualization of dendrimer molecules by transmission electron microscopy (TEM): Staining methods and Cryo-TEM of vitrified solutions. *Macromolecules* **31**, 6259–6265 (1998).
35. Yancey, D. F., Carino, E. V. & Crooks, R. M. Electrochemical synthesis and electrocatalytic properties of Au@Pt dendrimer-encapsulated nanoparticles. *J. Am. Chem. Soc.* **132**, 10988–10989 (2010).
36. Andersen, R. M., Yancey, D. F., Loussaert, J. A. & Crooks, R. M. Multistep galvanic exchange synthesis yielding fully reduced Pt dendrimer-encapsulated nanoparticles. *Langmuir* **30**, 15009–15015 (2014).
37. Li, N., Zhao, P. & Astruc, D. Anisotropic gold nanoparticles: synthesis, properties, applications, and toxicity. *Angew. Chem. Int. Ed. Engl.* **52**, 1756–1789 (2014).
38. Wunder, S., Lu, Y., Albrecht, M. & Ballauff, M. Catalytic activity of faceted gold nanoparticles studied by a model reaction: evidence for substrate-induced surface restructuring. *ACS Catal.* **1**, 908–916 (2011).
39. Gu, S., Wunder, S., Lu, Y. & Ballauff, M. Kinetic analysis of the catalytic reduction of 4-nitrophenol by metallic nanoparticles. *J. Phys. Chem. C* **118**, 18618–18625 (2014).
40. Aditya, T., Pal, A. & Pal, T. Nitroarene reduction: a trusted model reaction to test nanoparticle catalysts. *Chem. Commun.* **51**, 9410–9431 (2015).
41. Zhao, P., Feng, X., Huang, D., Yang, G. & Astruc, D. Basic concepts and recent advances in nitrophenol reduction by gold- and other transition metal nanoparticles. *Coord. Chem. Rev.* **287**, 114–136 (2015).
42. Gu, S., Lu, Y., Kaiser, J., Albrecht, M. & Ballauff, M. Kinetic analysis of the reduction of 4-nitrophenol catalyzed by Au/Pd nanoalloys immobilized in spherical polyelectrolyte brushes. *Phys. Chem. Chem. Phys.* **17**, 28137–28143 (2015).
43. Alonso, F., Moglie, Y. & Radivoy, G. Copper nanoparticles in click chemistry. *Acc. Chem. Res.* **48**, 2516–2528 (2015).
44. Ostwald, W. Studien über die Bildung und Umwandlung fester Körper. *Z. Phys. Chem.* **22**, 289–330 (1897).
45. Salavati-Niasari, M. & Davar, F. Synthesis of copper (I) oxide nanoparticles by thermal decomposition of a new precursor. *Mater. Lett.* **63**, 441–443 (2009).
46. Biesinger, M. C., Lau, L. W. M., Gerson, A. R. & Smart, R. S. C. Resolving surface chemical states in XPS analysis of first row transition metals, oxides and hydroxides: Sc, Ti, V, Cu and Zn. *Appl. Surf. Sci.* **257**, 887–898 (2010).
47. Wang, C. *et al.* Highly efficient transition metal nanoparticle catalysts in aqueous solutions. *Angew. Chem. Int. Ed. Engl.* **55**, 3091–3095 (2016).
48. Polshettiwar, V. & Varma, R. S. Green chemistry by nanocalysis. *Green Chem.* **12**, 743–754 (2010).

## Acknowledgements

Helpful discussions with Dr Jun Zhang (Univ. Chongqing) and Professors Nathalie Audebrand and Jean-René Hamon (Univ. Rennes 1), and financial support from the China Scholarship Council (CSC, grant to XL), the Universities of Bordeaux, Rennes 1 and San Sebastian, CIC biomaGUNE, MAT2013-48169-R (Spanish Ministry of Economy, MINECO), and H2020-MSCA-RISE-2014 HYMADE (project number 645686) are gratefully acknowledged.

## Author contributions

X.L., D.G., S.M., P.H., J.R. and D.A. conceived the experiments and wrote the paper. The experiments were performed by X.L. (chemistry), J.I. and R.C. (TEM and EDX) and D.G. (XPS).

## Additional information

**Supplementary Information** accompanies this paper at <http://www.nature.com/naturecommunications>

**Competing financial interests:** The authors declare no competing financial interests.

**Reprints and permission** information is available online at <http://npg.nature.com/reprintsandpermissions/>

**How to cite this article:** Liu, X. *et al.* Precise localization of metal nanoparticles in dendrimer nanosnakes or inner periphery and consequences in catalysis. *Nat. Commun.* **7**, 13152 doi: 10.1038/ncomms13152 (2016).



This work is licensed under a Creative Commons Attribution 4.0 International License. The images or other third party material in this article are included in the article's Creative Commons license, unless indicated otherwise in the credit line; if the material is not included under the Creative Commons license, users will need to obtain permission from the license holder to reproduce the material. To view a copy of this license, visit <http://creativecommons.org/licenses/by/4.0/>

© The Author(s) 2016